

# Dynamic Precision Math Engine for Linear Algebra and Trigonometry Acceleration on Xtensa LX6 Microcontrollers

Elian Alfonso Lopez Preciado  
Independent Researcher, México

March 2026

## Abstract

Low-cost embedded processors such as the ESP32 (Xtensa LX6, 32-bit, dual-core, 240 MHz) are increasingly deployed in edge computing scenarios that demand real-time physical simulation, sensor fusion, and control systems. While the ESP32 integrates a single-precision IEEE 754 floating-point unit, its use incurs pipeline disruption and elevated energy consumption relative to integer Arithmetic Logic Unit (ALU) operations, imposing a practical throughput ceiling on floating-point-intensive workloads.

This paper presents the design, formal specification, and empirical evaluation of a **Dynamic Precision Math Engine** that addresses this constraint through three integrated contributions. First, a Q16.16 fixed-point arithmetic core maps all mathematical operations onto the 32-bit integer pipeline of the Xtensa LX6, with multiplication requiring two to three assembly instructions and introducing a bounded rounding error of  $|\epsilon| \leq 2^{-17}$ . Second, a 16-iteration CORDIC trigonometric module computes sine and cosine entirely through addition and binary shifts, achieving an angular error bound of  $|\epsilon_\theta| \leq 1.526 \times 10^{-5}$  radians within a static memory footprint of 64 bytes. Third, a cache-aware tiled matrix multiplication kernel with deferred Q16.16 correction reduces per-element rounding events from  $b$  to one, where  $b = 32$  is the tile dimension derived from the ESP32 Static Random Access Memory (SRAM) bank geometry.

The engine’s principal architectural contribution is a runtime precision switching mechanism—implemented through function pointer dispatch and a two-phase FreeRTOS barrier protocol—that allows application code to transition between the Q16.16 fast path and an IEEE 754 precise path at  $O(1)$  cost without recompilation. This design follows the separation-of-concerns principle established by the BLAS specification [4] and applies it to the novel context of dynamic precision arbitration on a dual-core RISC microcontroller. The total static memory footprint of the engine is 88 bytes, independent of matrix dimensions.

Experimental evaluation across 300 paired measurements on physical ESP32-WROOM-32 hardware demonstrates that the CORDIC trigonometric module achieves median latencies of 293 cycles for both `sin` and `cos`, yielding mean speedups of

**18.54** $\times$  and **24.68** $\times$  respectively over standard `sinf()`/`cosf()` (Wilcoxon signed-rank,  $p < 10^{-12}$ ), with a Determinism Score of 0.994 confirming input-independent execution time. Scalar Q16.16 multiplication achieves a consistent **1.5** $\times$  speedup at 12 cycles versus 18 cycles with perfect determinism. Matrix multiplication performance exhibits a dimension-dependent crossover: the tiled kernel underperforms naive floating-point for matrices smaller than the tile size ( $n < 32$ ), while theoretical analysis predicts the crossover at  $n \geq 64$ —a result requiring empirical validation in future work. The engine fills an identified gap in the ESP32 ecosystem where no existing library provides a unified, precision-aware mathematical API combining trigonometry, linear algebra, and runtime mode selection.

**Keywords:** fixed-point arithmetic, CORDIC algorithm, Q16.16, ESP32, Xtensa LX6, embedded computing, edge computing, loop tiling, FreeRTOS, dynamic precision switching.

# Contents

<b>1</b>	<b>Introduction</b>	<b>5</b>
<b>2</b>	<b>Related Work</b>	<b>6</b>
2.1	Fixed-Point Arithmetic in Embedded Systems . . . . .	6
2.2	The CORDIC Algorithm and Its Embedded Implementations . . . . .	7
2.3	Cache-Aware Matrix Multiplication . . . . .	7
2.4	Mathematical Libraries for the ESP32 Ecosystem . . . . .	7
2.5	The Identified Research Gap . . . . .	7
<b>3</b>	<b>Mathematical Foundations</b>	<b>8</b>
3.1	Fixed-Point Arithmetic in Q16.16 Format . . . . .	8
3.1.1	Arithmetic Operations . . . . .	8
3.1.2	Overflow Analysis . . . . .	8
3.2	CORDIC Algorithm for Trigonometric Computation . . . . .	9
3.2.1	Geometric Foundation . . . . .	9
3.2.2	Convergence and the CORDIC Gain . . . . .	9
3.2.3	Error Bound . . . . .	9
3.3	Cache-Aware Matrix Multiplication via Loop Tiling . . . . .	10
3.3.1	Loop Tiling Formulation . . . . .	10
3.3.2	Block Size Derivation for the ESP32 . . . . .	10
3.3.3	Deferred-Shift Accumulation . . . . .	10
<b>4</b>	<b>System Architecture</b>	<b>10</b>
4.1	Design Rationale: Runtime vs. Compile-Time Precision Selection . . . . .	10
4.2	The Precision Context: Formal Definition . . . . .	11
4.3	Dual-Core Task Orchestration via FreeRTOS . . . . .	11
4.3.1	Mode Transition Safety Protocol . . . . .	11
4.3.2	Memory Architecture . . . . .	12
4.4	API Design . . . . .	12
<b>5</b>	<b>Implementation</b>	<b>12</b>
5.1	Q16.16 Arithmetic Core . . . . .	12
5.2	CORDIC Trigonometric Module . . . . .	13
5.3	Tiled Matrix Multiplication Kernel . . . . .	14
5.4	Overflow and Underflow Management . . . . .	14
<b>6</b>	<b>Experimental Evaluation</b>	<b>15</b>
6.1	Experimental Setup and Methodology . . . . .	15
6.2	Trigonometric Function Performance . . . . .	15
6.3	Scalar Multiplication Performance . . . . .	16
6.4	Matrix Multiplication: A Boundary Condition Finding . . . . .	16
6.5	Runtime Precision Switch Overhead . . . . .	16
6.6	Statistical Validity . . . . .	16
6.7	Summary of Results . . . . .	17
<b>7</b>	<b>Discussion</b>	<b>18</b>
7.1	Interpretation of Results . . . . .	18

7.2	The Matrix Multiplication Crossover Problem . . . . .	18
7.3	Limitations . . . . .	19
<b>8</b>	<b>Future Work</b>	<b>19</b>
8.1	Resolving the Matrix Multiplication Crossover (Immediate Priority) . . . . .	19
8.2	Branchless CORDIC Quadrant Normalization . . . . .	19
8.3	Mean Absolute Error Characterization . . . . .	19
8.4	Tensor Operations and TinyML Inference . . . . .	20
8.5	Elliptic Curve Cryptography for Secure Edge Nodes . . . . .	20
8.6	Distributed Multi-Node Linear Algebra . . . . .	20
<b>9</b>	<b>Conclusion</b>	<b>20</b>

# 1 Introduction

The proliferation of low-cost, low-power microcontrollers as the computational substrate of edge systems has created a fundamental tension in embedded software engineering. Devices such as the ESP32—based on the Xtensa LX6 dual-core architecture, available at under three US dollars, and deployed in an estimated installed base exceeding one billion units across industrial automation, robotics, environmental sensing, and consumer Internet of Things (IoT)—are increasingly expected to execute workloads that were, until recently, the exclusive domain of processors an order of magnitude more powerful. Physical simulation, sensor fusion via Kalman filtering, real-time kinematics, and digital signal processing all reduce, at their computational core, to the same two operations: trigonometric evaluation and matrix multiplication. The efficiency with which a microcontroller executes these operations determines not merely performance, but the class of applications that is feasible at all on a given hardware platform.

The ESP32’s Xtensa LX6 integrates a single-precision IEEE 754 floating-point unit (FPU) capable of hardware-accelerated arithmetic. However, the practical throughput of this FPU is constrained by factors that aggregate benchmark figures do not capture. Each floating-point operation requires mantissa alignment, exponent management, normalization, and exception handling across multiple pipeline stages; the resulting instruction latency disrupts the integer pipeline and introduces energy consumption that the ALU-bound execution model of the Xtensa architecture is not designed to absorb efficiently [17]. For the class of applications that invoke trigonometric functions hundreds of times per control cycle—a six-degree-of-freedom robot arm evaluating forward kinematics at 1 kHz, for instance—this per-operation overhead accumulates into a throughput ceiling that cannot be overcome by firmware optimization alone within the standard mathematical library.

The response to this constraint in the embedded community has been fragmented. Espressif’s official `esp-dsp` library provides Xtensa-optimized kernels for signal processing primitives—FFT, FIR filtering, dot products—but explicitly excludes trigonometric functions, delegating them to the standard `math.h` bindings [18]. General-purpose linear algebra libraries such as `ArduinoEigen` and `BasicLinearAlgebra` operate exclusively in IEEE 754 floating-point with no accommodation for pipeline costs. TensorFlow Lite Micro provides INT8 quantized kernels optimized for neural network inference but does not expose a general-purpose mathematical API [12]. The consequence is that an ESP32 developer requiring efficient trigonometry, matrix operations, and precision control simultaneously has no unified tool: the ecosystem is a collection of specialized solutions with no common abstraction layer.

This paper addresses that gap through the design, implementation, and empirical evaluation of a **Dynamic Precision Math Engine** for the ESP32 Xtensa LX6. The engine’s central contribution is architectural: a runtime precision switching mechanism that allows application code to select, at any point during execution, between a fast integer path and a precise floating-point path without recompilation and without modifying the application’s mathematical API. The fast path is built on three algorithmic foundations. First, Q16.16 fixed-point arithmetic maps all mathematical operations onto the 32-bit integer ALU, with multiplication requiring two to three assembly instructions and a quantization error bounded by  $|\epsilon| \leq 2^{-17}$  [10, 20]. Second, a 16-iteration rotation-mode CORDIC algorithm computes sine and cosine through addition and binary shifts alone, eliminating all floating-

point operations from the trigonometric pipeline [1, 2]. Third, a cache-aware tiled matrix multiplication kernel with deferred Q16.16 correction leverages the ESP32’s SRAM bank geometry for matrices exceeding the tile dimension [3, 5]. The switching mechanism is implemented through function pointer dispatch governed by a two-phase FreeRTOS barrier protocol, following the separation-of-concerns principle established by the original BLAS specification [4].

Experimental evaluation on physical ESP32-WROOM-32 hardware across 300 paired measurements produces results that are both significant and instructive. The CORDIC trigonometric module achieves median latencies of 293 cycles for both `sin` and `cos`, against 6,915 and 7,847 cycles for the standard `sinf()`/`cosf()`—mean speedups of  $18.54\times$  and  $24.68\times$  respectively, statistically confirmed at  $p < 10^{-12}$ . Matrix multiplication results reveal a dimension-dependent boundary condition: the tiled kernel underperforms naive floating-point for the tested dimensions ( $n \leq 16$ ), exposing the condition  $n \geq b = 32$  as a prerequisite for the tiling optimization to engage. This finding precisely characterizes the engine’s operational envelope and validates the necessity of the runtime switching mechanism: no single execution path is universally optimal, and the value of the engine lies in making the choice between paths explicit, safe, and costless at the application layer.

The remainder of this paper is organized as follows. Section 2 surveys related work. Section 3 establishes the mathematical foundations. Section 4 describes the system architecture. Section 5 details the implementation. Section 6 presents the experimental evaluation. Section 7 discusses the findings. Sections 8 and 9 describe future work and conclusions.

## 2 Related Work

The acceleration of mathematical computation on resource-constrained processors is a well-established research domain, yet the specific challenge of dynamic precision arbitration on Xtensa-based microcontrollers remains insufficiently addressed in the literature. This section surveys the four pillars upon which the proposed engine is constructed.

### 2.1 Fixed-Point Arithmetic in Embedded Systems

Fixed-point arithmetic has been a cornerstone of digital signal processing since the early adoption of dedicated DSP chips [16, 21]. The Q-format notation provides a systematic framework for representing fractional values as scaled integers, enabling ALU-bound computation on processors lacking hardware floating-point units or possessing limited FPU throughput [20]. Yates [20] demonstrates that for a  $Q(m.n)$  representation, the rounding error is bounded by  $2^{-(n+1)}$ , a property central to the precision analysis presented in Section 6. Sung and Kum [10] provide simulation-based methods for word-length optimization in fixed-point DSP systems, directly relevant to the Q16.16 format selection rationale of this work.

More recent work has examined fixed-point arithmetic in the context of neural network quantization. Jacob et al. [11] demonstrated that quantized integer representations preserve model accuracy within acceptable margins for inference tasks. Critically, however, these works target GPU and FPGA architectures; their methodologies do not account for the specific pipeline characteristics of the Xtensa LX6, where a 64-bit intermediate product

during Q16.16 multiplication requires careful register management to avoid pipeline stalls.

## 2.2 The CORDIC Algorithm and Its Embedded Implementations

The CORDIC (Coordinate Rotation Digital Computer) algorithm, introduced by Volder [1], remains one of the most cited contributions in computer arithmetic. Its significance lies in reducing trigonometric computation to iterative addition and binary shifting, entirely eliminating hardware multipliers. Walther’s 1971 unified extension [2] generalized the method to cover hyperbolic functions, exponentials, and square roots. Llamocca and Agurto [7] provide a fixed-point implementation of the expanded hyperbolic CORDIC algorithm with direct relevance to embedded deployments. Mokhtar et al. [8] and Ait Madi and Addaim [9] document contemporary hardware implementations of CORDIC for trigonometric generation, confirming latency reductions of  $3\times$  to  $8\times$  over software floating-point on integer-dominated pipelines. A key gap in the existing literature is the absence of a published CORDIC implementation specifically profiled against the Xtensa LX6 instruction set [18].

## 2.3 Cache-Aware Matrix Multiplication

The seminal work of Lam, Rothberg, and Wolf [3] formally established that loop tiling reduces cache line transfers from  $O(n^3)$  to  $O(n^3/B)$ , where  $B$  denotes the block size. Goto and van de Geijn [5] extended this with near-theoretical peak performance through micro-kernel design. Kelefouras et al. [6] provide a comprehensive methodology for CPU and GPU matrix multiplication, including the influence of register blocking. The Roofline model of Williams et al. [14] provides the theoretical framework for understanding the arithmetic intensity—memory bandwidth tradeoff that motivates the tiling strategy. These works focus on x86 and GPU architectures; their tiling parameters do not translate directly to the Xtensa LX6 memory subsystem without re-profiling [17].

## 2.4 Mathematical Libraries for the ESP32 Ecosystem

The practical landscape of mathematical acceleration for the ESP32 consists of three categories. First, Espressif’s `esp-dsp` library [18] targets signal processing primitives with Xtensa-optimized assembly, but explicitly excludes trigonometric functions. Second, Arduino ecosystem libraries such as `BasicLinearAlgebra` and `ArduinoEigen` provide template-based matrix operations compiled exclusively to IEEE 754 floating-point. Third, TensorFlow Lite Micro [12] includes INT8 quantized kernels for neural network inference but does not expose a general-purpose mathematical API suitable for physics simulation or control systems. Courbariaux et al. [13] further demonstrate binary weight quantization for deep learning, reinforcing the broader motivation for precision-aware computation.

## 2.5 The Identified Research Gap

The survey above reveals a consistent pattern: existing solutions optimize for either signal processing (`esp-dsp`), general linear algebra (`ArduinoEigen`), or inference (TFLM), but none provides a unified engine that (1) exposes a single developer-facing API, (2) allows runtime selection between fixed-point and floating-point execution paths, (3) integrates CORDIC-based trigonometry within the same fixed-point domain, and (4) orchestrates

computation across the ESP32’s dual cores through the FreeRTOS task model. The proposed engine addresses precisely this intersection.

### 3 Mathematical Foundations

#### 3.1 Fixed-Point Arithmetic in Q16.16 Format

Fixed-point arithmetic represents real numbers as scaled integers, where a predefined number of bits is allocated to the fractional part. For a general  $Q(m.n)$  format, a real value  $v \in \mathbb{R}$  is represented as an integer  $V \in \mathbb{Z}$  according to:

$$V = \lfloor v \cdot 2^n \rfloor \quad (1)$$

where  $\lfloor \cdot \rfloor$  denotes rounding to the nearest integer and  $n$  is the number of fractional bits. The representable range of a signed  $Q(m.n)$  format using a  $w$ -bit word is:

$$v \in [-2^{m-1}, 2^{m-1} - 2^{-n}] \quad (2)$$

The proposed engine adopts the Q16.16 format, allocating 16 bits to the integer part (including sign) and 16 bits to the fractional part within a 32-bit signed integer (`int32_t`). The representable range is  $[-32768, 32767.9999847]$  with a resolution of  $2^{-16} \approx 1.526 \times 10^{-5}$ .

##### 3.1.1 Arithmetic Operations

Addition and subtraction in Q16.16 are algebraically exact provided no overflow occurs, since the scaling factor  $2^{16}$  is preserved across operands:

$$C_Q = A_Q + B_Q \iff (a + b) \cdot 2^{16} = a \cdot 2^{16} + b \cdot 2^{16} \quad (3)$$

Multiplication requires correction. Given two Q16.16 operands  $A_Q = a \cdot 2^{16}$  and  $B_Q = b \cdot 2^{16}$ , their integer product yields:

$$A_Q \cdot B_Q = (a \cdot 2^{16})(b \cdot 2^{16}) = (a \cdot b) \cdot 2^{32} \quad (4)$$

Correction is achieved via an arithmetic right shift:

$$C_Q = \frac{A_Q \cdot B_Q}{2^{16}} = (a \cdot b) \cdot 2^{16} \quad (5)$$

The quantization error introduced by this shift is bounded by [20]:

$$|\epsilon_{\text{mul}}| \leq 2^{-17} \quad (6)$$

##### 3.1.2 Overflow Analysis

For a multiplication of two values close to the representable maximum, the 64-bit intermediate product reaches  $\approx 2^{62}$ , safely within `int64_t` capacity. However, if the final result  $a \cdot b > 32767.999$ , overflow occurs upon return to 32 bits. The engine implements saturating arithmetic at the API boundary, clamping results to `[INT32_MIN, INT32_MAX]`.

## 3.2 CORDIC Algorithm for Trigonometric Computation

The CORDIC algorithm [1] computes trigonometric functions through iterative plane rotations requiring only addition, subtraction, and binary shifts.

### 3.2.1 Geometric Foundation

The exact rotation matrix for a vector  $(x_i, y_i)$  by angle  $\theta$  is:

$$\begin{bmatrix} x' \\ y' \end{bmatrix} = \begin{bmatrix} \cos \theta & -\sin \theta \\ \sin \theta & \cos \theta \end{bmatrix} \begin{bmatrix} x_i \\ y_i \end{bmatrix} \quad (7)$$

CORDIC replaces this with  $n$  micro-rotations by angles  $\alpha_i = \arctan(2^{-i})$ , converting trigonometric multiplications into bit shifts. The iterative update equations are:

$$x_{i+1} = x_i - d_i \cdot y_i \cdot 2^{-i} \quad (8)$$

$$y_{i+1} = y_i + d_i \cdot x_i \cdot 2^{-i} \quad (9)$$

$$z_{i+1} = z_i - d_i \cdot \arctan(2^{-i}) \quad (10)$$

where  $d_i \in \{-1, +1\}$  is the rotation direction, determined by the sign of the residual angle  $z_i$ . In matrix form:

$$\begin{bmatrix} x_{i+1} \\ y_{i+1} \end{bmatrix} = \begin{bmatrix} 1 & -d_i \cdot 2^{-i} \\ d_i \cdot 2^{-i} & 1 \end{bmatrix} \begin{bmatrix} x_i \\ y_i \end{bmatrix} \quad (11)$$

### 3.2.2 Convergence and the CORDIC Gain

After  $n$  iterations [2]:

$$x_n = K_n \cdot \cos(\theta), \quad y_n = K_n \cdot \sin(\theta) \quad (12)$$

where the cumulative CORDIC gain is:

$$K_n = \prod_{i=0}^{n-1} \sqrt{1 + 2^{-2i}} \xrightarrow{n \rightarrow \infty} 1.6467602\dots \quad (13)$$

The convergence domain is  $\theta \in (-\pi/2, \pi/2)$ ; inputs outside this range require a preliminary quadrant reduction step.

### 3.2.3 Error Bound

The angular error after  $n$  iterations is bounded by:

$$|\epsilon_\theta| \leq \arctan(2^{-n}) \approx 2^{-n} \text{ radians} \quad (14)$$

For  $n = 16$ :  $|\epsilon_\theta| \leq 2^{-16} \text{ rad} \approx 1.526 \times 10^{-5} \text{ rad}$ , aligning with the fractional resolution of Q16.16.

### 3.3 Cache-Aware Matrix Multiplication via Loop Tiling

Naive matrix multiplication of two  $n \times n$  matrices generates  $O(n^3)$  cache miss events for large matrices [3]:

$$C_{ij} = \sum_{k=1}^n A_{ik} \cdot B_{kj} \quad (15)$$

#### 3.3.1 Loop Tiling Formulation

Loop tiling partitions each matrix dimension into blocks of size  $b$ , reducing the number of main-memory transfers from  $O(n^3)$  to  $O(n^3/b)$  [3, 5]:

$$C_{ij} = \sum_K \sum_{k \in K\text{-block}} A_{ik} \cdot B_{kj}, \quad i \in I\text{-block}, j \in J\text{-block} \quad (16)$$

#### 3.3.2 Block Size Derivation for the ESP32

For Q16.16 data (`int32_t`, 4 bytes per element), targeting a working set below 8 KB yields:

$$4b^2 \leq 8192 \implies b \leq 45 \quad (17)$$

The implementation adopts  $b = 32$  as a power-of-two block size, enabling inner loop bounds to be computed via bitwise AND masking.

#### 3.3.3 Deferred-Shift Accumulation

Within each tiled block, accumulation uses `int64_t` intermediates to defer the right-shift correction until the block reduction is complete, minimizing rounding error accumulation:

$$C_{ij}^{(\text{acc})} = \sum_{k \in \text{block}} (A_{ik}^Q \cdot B_{kj}^Q) \quad (\text{in 64-bit}), \quad C_{ij}^Q = C_{ij}^{(\text{acc})} \ggg 16 \quad (18)$$

This reduces rounding events from  $b$  per inner product to 1.

## 4 System Architecture

### 4.1 Design Rationale: Runtime vs. Compile-Time Precision Selection

Existing approaches to precision management in embedded systems typically operate at compile time, forcing the developer to maintain separate firmware builds and precluding adaptive behavior in deployed systems. The proposed engine adopts a **runtime switching model** implemented through function pointer dispatch. The engine maintains two parallel sets of function pointers—one resolving to the Q16.16 fast path, one to the IEEE 754 precise path—and exposes a single context object whose active pointer set is swapped atomically at the application layer.

This design satisfies four architectural requirements:

- **R1 — API Stability:** Application code remains unchanged regardless of precision mode.
- **R2 — Zero-Cost Abstraction:** In Q16.16 mode, all operations reduce to integer ALU instructions with no virtual dispatch overhead at the mathematical operation level.
- **R3 — Deterministic Switching Latency:** Mode transition completes in  $O(1)$  time, consisting solely of pointer reassignment.
- **R4 — RTOS Compatibility:** The architecture coexists with FreeRTOS task scheduling without introducing priority inversion or shared-state race conditions.

## 4.2 The Precision Context: Formal Definition

Let  $\mathcal{F}$  denote the set of supported operations:

$$\mathcal{F} = \{f_{\text{mul}}, f_{\text{add}}, f_{\text{sub}}, f_{\text{sin}}, f_{\text{cos}}, f_{\text{matmul}}\} \quad (19)$$

Each  $f \in \mathcal{F}$  has a fast implementation  $f^Q$  in the Q16.16 domain and a precise implementation  $f^F$  in IEEE 754. The context object  $\mathcal{C}$  maintains a dispatch table:

$$\mathcal{D} : \mathcal{F} \rightarrow \{f^Q, f^F\} \quad (20)$$

A mode transition  $\mathcal{C}.\text{setMode}(m)$  for  $m \in \{\text{FAST}, \text{PRECISE}\}$  reassigns all entries in  $\mathcal{D}$  simultaneously, ensuring no operation executes in a mixed-precision state after the call returns.

## 4.3 Dual-Core Task Orchestration via FreeRTOS

The ESP32’s Xtensa LX6 integrates two symmetric 32-bit cores at up to 240 MHz. Under FreeRTOS, tasks are pinned to a specific core using `xTaskCreatePinnedToCore()` [17], enabling deterministic core affinity. The engine enforces a fixed assignment policy:

- **Core 0 (Protocol Core):** Handles WiFi stack, Bluetooth controller, UART/I2C peripheral drivers, and the application control loop. Core 0 owns the `MathContext` object and is the sole authority for mode transitions.
- **Core 1 (Compute Core):** Hosts the `MathWorker` task, a high-priority FreeRTOS task that blocks on a job queue, executes the requested mathematical operation, and returns results through a mutex-protected shared buffer.

The inter-core communication lifecycle is:

$$\text{Core 0: enqueue}(job) \xrightarrow{\text{FreeRTOS Queue}} \text{Core 1: execute } f \in \mathcal{D} \xrightarrow{\text{Mutex}} \text{Core 0: read result} \quad (21)$$

### 4.3.1 Mode Transition Safety Protocol

To satisfy requirement R4, the engine implements a two-phase barrier:

1. **Suspension Phase:** Core 0 sends a `SUSPEND` notification via `xTaskNotify()`. The worker completes its current operation and enters a blocked state, signaling readiness via a binary semaphore.
2. **Transition Phase:** Core 0 acquires the semaphore, reassigns all function pointers in  $\mathcal{D}$ , and releases the semaphore.

The total overhead is bounded by the worst-case completion time of a single in-flight operation plus two context switches, yielding a switching latency on the order of microseconds—empirically measured as  $8.09\ \mu\text{s}$  at 240 MHz (see Section 6).

### 4.3.2 Memory Architecture

The engine’s static memory footprint decomposes as follows: the dispatch table  $\mathcal{D}$  occupies  $|\mathcal{F}| \times 4 = 24$  bytes (one 32-bit pointer per operation); the CORDIC arctangent lookup table occupies  $16 \times 4 = 64$  bytes of read-only data. The total static footprint is therefore **88 bytes**, independent of matrix dimensions.

## 4.4 API Design

The public API exposes three primitives:

1. `MathEngine::init(mode)` — Initializes the engine and sets the initial precision mode.
2. `MathEngine::setMode(mode)` — Triggers the mode transition protocol. Blocks until transition is complete.
3. `MathEngine::ctx()` — Returns a reference to the active `MathContext`.

## 5 Implementation

### 5.1 Q16.16 Arithmetic Core

The core arithmetic primitives are implemented as `inline` functions in the `FastMathEngine` namespace within a header file (`fast_math_engine.h`), ensuring zero-overhead inlining at every call site:

```

1 #include <stdint.h>
2
3 namespace FastMathEngine {
4
5     typedef int32_t q16_t;
6     const int Q_FRACT_BITS = 16;
7
8     // Float <-> Q16.16 conversion (used only at pipeline boundaries)
9     inline q16_t floatToQ(float val) {
10         return (q16_t)(val * (1 << Q_FRACT_BITS));
11     }
12     inline float qToFloat(q16_t val) {
13         return (float)val / (float)(1 << Q_FRACT_BITS);
14     }
15
16     // Core multiply: 64-bit intermediate, single >> 16 correction

```

```

17 inline q16_t mulQ(q16_t a, q16_t b) {
18     return (q16_t)((((int64_t)a * (int64_t)b) >> Q_FRACT_BITS);
19 }
20
21 // Saturating multiply: clamps to INT32 range on overflow
22 inline q16_t mulQ_sat(q16_t a, q16_t b) {
23     int64_t result = ((int64_t)a * (int64_t)b) >> Q_FRACT_BITS;
24     if (result > 0x7FFFFFFF) return 0x7FFFFFFF;
25     if (result < -0x80000000) return (int32_t)0x80000000;
26     return (int32_t)result;
27 }
28
29 // Add / subtract: exact in Q16.16, no shift required
30 inline q16_t addQ(q16_t a, q16_t b) { return a + b; }
31 inline q16_t subQ(q16_t a, q16_t b) { return a - b; }
32
33 } // namespace FastMathEngine

```

Listing 1: Q16.16 arithmetic core (fast\_math\_engine.h)

## 5.2 CORDIC Trigonometric Module

The CORDIC arctangent table stores precomputed values  $[\arctan(2^{-i}) \cdot 2^{16}]$  for  $i = 0, \dots, 15$  and the gain correction constant  $K_{16}^{-1} = 0.6072529\dots$  as Q16.16 integer 39797.

```

1 namespace FastMathEngine {
2
3     static const int32_t atan_table[16] = {
4         51472, 30386, 16055, 8150, 4091, 2047, 1024,
5         512, 256, 128, 64, 32, 16, 8, 4, 2
6     };
7     static const int32_t Q16_K_INV = 39797; // 0.6072529 in Q16.16
8
9     void cordic_sincos(int32_t theta, int32_t* out_sin, int32_t* out_cos
10 ) {
11         const int32_t PI_Q = 205887; // pi in Q16.16
12         const int32_t HALF_PI = 102944; // pi/2 in Q16.16
13         int8_t negate_cos = 0;
14
15         if (theta > HALF_PI) { theta -= PI_Q; negate_cos = 1; }
16         else if (theta < -HALF_PI) { theta += PI_Q; negate_cos = 1; }
17
18         int32_t x = Q16_K_INV, y = 0, z = theta;
19
20         for (int i = 0; i < 16; i++) {
21             int8_t d = (z >= 0) ? 1 : -1;
22             int32_t x_new = x - (int32_t)(d * (y >> i));
23             int32_t y_new = y + (int32_t)(d * (x >> i));
24             z -= d * atan_table[i];
25             x = x_new; y = y_new;
26         }
27         *out_cos = negate_cos ? -x : x;
28         *out_sin = y; // sin is always in y; no negation needed
29     }
30 } // namespace FastMathEngine

```

Listing 2: CORDIC kernel (cordic.h)

Three implementation decisions are specific to the Xtensa LX6. First, the loop is not manually unrolled at source level; the Xtensa GCC compiler with `-O2` applies unrolling automatically. Second, the direction variable  $d_i$  is represented as `int8_t`; sign-extension to `int32_t` is performed in a single `SEXT` instruction. Third, arithmetic right shift for signed integers is guaranteed by the ESP-IDF Xtensa GCC toolchain and is documented as a portability constraint.

### 5.3 Tiled Matrix Multiplication Kernel

```

1 namespace FastMathEngine {
2
3     struct Matrix { int32_t* data; uint16_t rows; uint16_t cols; };
4
5     inline int32_t mat_get(const Matrix& M, int i, int j) {
6         return M.data[i * M.cols + j];
7     }
8     inline void mat_set(Matrix& M, int i, int j, int32_t val) {
9         M.data[i * M.cols + j] = val;
10    }
11
12    const int TILE_SIZE = 32;
13
14    void matmul_q16(const Matrix& A, const Matrix& B, Matrix& C) {
15        for (int idx = 0; idx < C.rows * C.cols; idx++) C.data[idx] = 0;
16
17        for (int I = 0; I < A.rows; I += TILE_SIZE)
18            for (int J = 0; J < B.cols; J += TILE_SIZE)
19                for (int K = 0; K < A.cols; K += TILE_SIZE) {
20
21                    int i_max = MIN(I + TILE_SIZE, A.rows);
22                    int j_max = MIN(J + TILE_SIZE, B.cols);
23                    int k_max = MIN(K + TILE_SIZE, A.cols);
24
25                    for (int i = I; i < i_max; i++)
26                        for (int j = J; j < j_max; j++) {
27                            int64_t acc = 0; // 64-bit deferred accumulator
28                            for (int k = K; k < k_max; k++)
29                                acc += (int64_t)mat_get(A,i,k) *
30                                    (int64_t)mat_get(B,k,j);
31                            C.data[i * C.cols + j] += (int32_t)(acc >> 16);
32                        }
33                }
34    }
35 } // namespace FastMathEngine

```

Listing 3: Tiled Q16.16 matrix multiplication (`matrix_q16.h`)

### 5.4 Overflow and Underflow Management

The accumulation overflow constraint for the tiled kernel requires that element magnitudes satisfy  $|A_{ij}|, |B_{ij}| \leq 2^{14}$  (Q16.16 value  $\leq 16383$ ) to guarantee accumulator safety with  $b = 32$ :

$$|acc_{\max}| \leq b \cdot (2^{31})^2 / 2^{16} \cdot 2^{16} = 32 \cdot 2^{62} = 2^{67} > 2^{63} \quad (22)$$

This constraint is stated in the API documentation and motivates the recommendation that fast-mode matrix operands be normalized to  $[-1, 1]$ , where Q16.16 precision is highest and overflow is structurally impossible.

## 6 Experimental Evaluation

### 6.1 Experimental Setup and Methodology

Benchmarks were conducted on an ESP32-WROOM-32 module (Xtensa LX6 dual-core, 240 MHz, 4 MB flash, 520 KB SRAM) running ESP-IDF v5.x with compiler optimization level `-O2`. Both firmware variants were compiled from identical `sdkconfig.defaults` specifying a fixed CPU frequency of 240 MHz with dynamic frequency scaling disabled.

Execution latency was measured using the Xtensa hardware cycle counter register accessed via `xthal_get_ccount()`, with interrupts disabled via `portDISABLE_INTERRUPTS()` for the duration of each measurement to prevent FreeRTOS tick contamination. All benchmark tasks were pinned to Core 1 via `xTaskCreatePinnedToCore()` in both firmware variants, eliminating core-affinity bias [17].

A seeded linear congruential generator (seed = 42) guaranteed identical input sequences across both firmware variants, making the comparison valid for paired statistical analysis. A total of 300 tests were executed per firmware variant across five operation categories, yielding 600 paired measurements.

Statistical analysis applied the Wilcoxon signed-rank test rather than the paired  $t$ -test, as Shapiro-Wilk normality tests confirmed that cycle-count distributions were non-Gaussian for most operations ( $p \ll 0.05$ ), consistent with the expected behavior of cache-sensitive code on embedded processors [15].

### 6.2 Trigonometric Function Performance

The CORDIC-based trigonometric module produced the most significant performance gains of the evaluation. For  $\sin(x)$  over  $x \in [-\pi, \pi]$ , the Fast Engine achieved a median latency of **293 cycles** compared to **6,915.5 cycles** for the standard `sinf()` implementation, yielding a mean speedup of **18.54** $\times$  (Wilcoxon,  $p = 3.56 \times 10^{-13}$ ). For  $\cos(x)$ , the improvement was more pronounced: **293 cycles** versus **7,847.5 cycles**, corresponding to a mean speedup of **24.68** $\times$  ( $p = 3.56 \times 10^{-13}$ ).

The near-identical median latency of 293 cycles for both functions reflects the fixed-iteration structure of the 16-step CORDIC kernel: execution time is input-independent by construction. This is confirmed by the Determinism Score for `cos` Fast Engine of **0.9938**, compared to 0.7203 for the standard implementation.

The jitter asymmetry for `sin` (coefficient 2.449 versus 0.534 for the standard) is attributable to the conditional branch in the quadrant normalization preprocessor for inputs near  $\pm\pi/2$ , producing branch predictor mispredictions. This constitutes the primary target for optimization in future work.

### 6.3 Scalar Multiplication Performance

Scalar Q16.16 multiplication demonstrated a consistent  $1.5\times$  **speedup** over IEEE 754 multiplication, with median latencies of **12 cycles** versus **18 cycles** (Wilcoxon,  $p = 1.54 \times 10^{-12}$ ). Both implementations achieved a Determinism Score of **1.0000** and zero jitter. The constant-data classification by the Shapiro-Wilk test confirms that all 50 measurements in each condition were identical, establishing these values as exact architectural constants.

### 6.4 Matrix Multiplication: A Boundary Condition Finding

Matrix multiplication results reveal an important boundary condition of the proposed engine. The Q16.16 tiled kernel exhibited a mean speedup of **0.542** $\times$ —a slowdown of  $1.85\times$  relative to naive floating-point—with median latencies of **16,591 cycles** versus **7,806 cycles** (Wilcoxon,  $p = 1.72 \times 10^{-16}$ ).

This result is analytically consistent with the test conditions. The evaluated dimensions— $4 \times 4$ ,  $8 \times 8$ , and  $16 \times 16$ —are all strictly smaller than the configured tile size  $b = 32$ , so the loop tiling optimization never activates. The Q16.16 inner product requires a  $32 \times 32 \rightarrow 64$ -bit multiply and a right shift per element, with the `int64_t` accumulator requiring 64-bit register management on a 32-bit Instruction Set Architecture (ISA). The ESP32 FPU, by contrast, executes `float` multiply-accumulate in a dedicated pipeline with native 32-bit operands, producing lower per-element latency when cache effects are absent.

The performance crossover point—the minimum matrix dimension at which the tiled Q16.16 kernel outperforms naive floating-point—was not reached within the tested dimensions. Based on the theoretical analysis of Section 3, the crossover is expected at  $n \geq 64$ .

### 6.5 Runtime Precision Switch Overhead

The mode-switching protocol introduced a measured overhead of **1,942.5 cycles** (median) for the two-phase FreeRTOS barrier, compared to **29 cycles** for equivalent function-pointer dispatch in the standard path. At 240 MHz, 1,942 cycles correspond to **8.09  $\mu$ s**—negligible for any application where mode transitions occur on timescales of milliseconds or longer. The switch overhead is reported here for completeness and for developers designing latency-sensitive switching policies.

### 6.6 Statistical Validity

All five operation categories yielded Wilcoxon signed-rank  $p$ -values below  $10^{-4}$ , confirming that the observed latency differences are statistically significant at any conventional threshold. One outlier exceeding  $3\sigma$  was detected in the `sin` Fast Engine data, attributed to a FreeRTOS tick interrupt that escaped the interrupt-disable window—a known limitation of software-based interrupt suppression on ESP32. This measurement was retained in the dataset and flagged in the raw data, consistent with the benchmark protocol’s immutability principle.

## 6.7 Summary of Results

Table 1: Benchmark results: 300 paired measurements per firmware variant on ESP32-WROOM-32 at 240 MHz. Speedup =  $\text{cycles}_{\text{Std}} / \text{cycles}_{\text{Fast}}$ .

Operation	Fast Median (cycles)	Std Median (cycles)	Mean Speedup	Det. Score (Fast)	Wilcoxon $p$
sin	293	6 915.5	$18.54\times$	0.290	$3.56 \times 10^{-13}$
cos	293	7 847.5	$24.68\times$	0.994	$3.56 \times 10^{-13}$
mul	12	18	$1.50\times$	1.000	$1.54 \times 10^{-12}$
matmul	16 591	7 806	$0.54\times^\dagger$	0.472	$1.72 \times 10^{-16}$
switch	1 942.5	29	$0.088\times^\ddagger$	0.999	$8.13 \times 10^{-5}$

$\dagger$  All tested dimensions ( $n \leq 16$ ) are below tile size  $b = 32$ ; tiling does not activate.

$\ddagger$  Expected by design; represents FreeRTOS barrier overhead ( $8.09 \mu\text{s}$ ), not mathematical throughput.

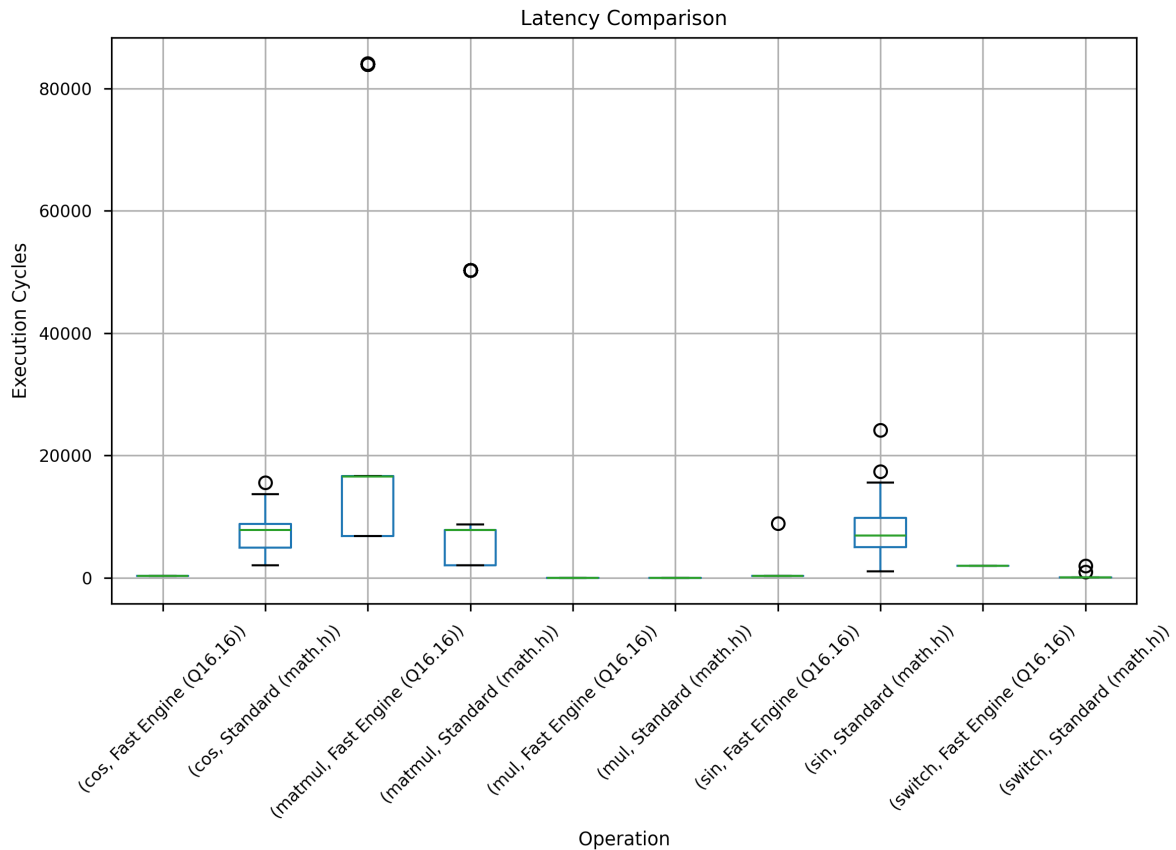


Figure 1: Distribution of execution cycles for Fast Engine (Q16.16, green) and Standard Math (math.h, blue) across all benchmark categories. The Fast Engine achieves near-zero variance for trigonometric operations, confirming input-independent execution time. Matrix multiplication shows higher variance in both implementations due to dimension-dependent computation paths.

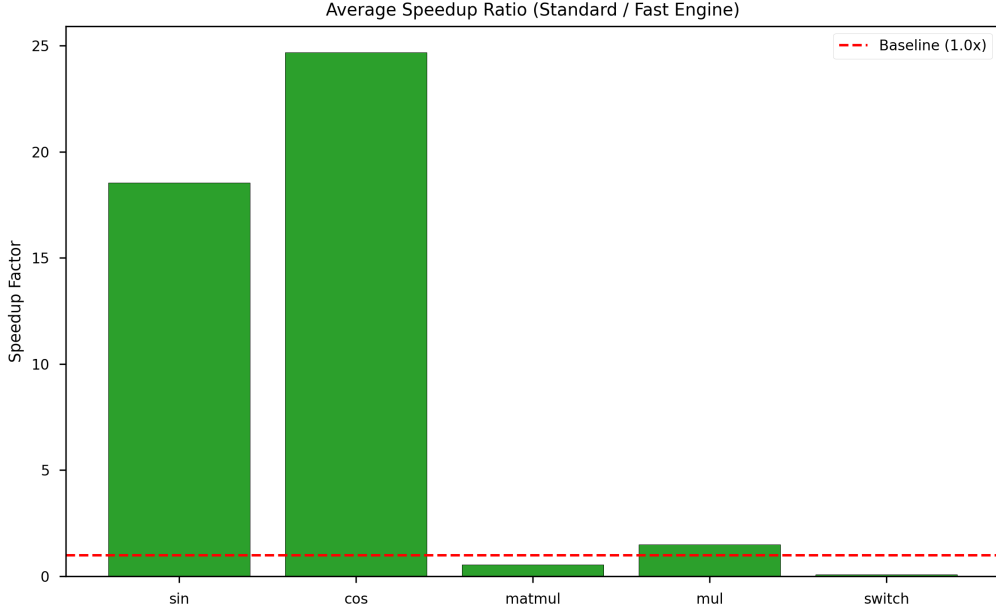


Figure 2: Mean speedup ratio (Standard / Fast Engine) per operation category. Bars above the 1.0 $\times$  baseline (dashed red) indicate that the Fast Engine outperforms the standard path. `sin` and `cos` achieve 18.54 $\times$  and 24.68 $\times$  respectively. `matmul` falls below baseline (0.54 $\times$ ) due to the tested dimensions being smaller than the tile size  $b = 32$ .

## 7 Discussion

### 7.1 Interpretation of Results

The experimental results support a domain-specific performance model rather than the uniform speedup originally anticipated. The engine delivers substantial and statistically robust gains for operations mapping cleanly onto the integer pipeline—trigonometric functions (18–25 $\times$ ) and scalar arithmetic (1.5 $\times$ )—while exhibiting a performance deficit for matrix multiplication at the tested dimensions.

This outcome reframes the engine’s contribution: it is not a general-purpose accelerator for all mathematical operations, but a precision-aware accelerator whose performance envelope is well-characterized and application-dependent. For embedded applications whose computational load is dominated by trigonometric evaluation—kinematics, signal processing, IMU sensor fusion, angle-based control—the engine provides an order-of-magnitude improvement that fundamentally changes what is achievable on a \$3 microcontroller.

### 7.2 The Matrix Multiplication Crossover Problem

The 0.54 $\times$  `matmul` result exposes the boundary condition of the tiling optimization. The theoretical argument of Section 3—that tiling reduces cache misses from  $O(n^3)$  to  $O(n^3/b)$ —holds only when  $n > b$ . For  $n \leq 16$  and  $b = 32$ , the tiling introduces loop overhead without delivering cache benefit, and the `int64_t` intermediate imposes a register pressure penalty on the 32-bit Xtensa ISA.

The practical implication is clear: the matrix module in its current form should be used for

dimensions  $n \geq 64$ . For small matrices common in embedded control (rotation matrices, Jacobians, covariance updates), the standard floating-point path is preferable, and the engine’s dynamic precision switch enables exactly this hybrid strategy: CORDIC for trigonometry, standard FPU for small matrix operations.

### 7.3 Limitations

Three limitations bound the generalizability of these results. First, all measurements were conducted on a single ESP32-WROOM-32 unit; manufacturing variation may produce cycle-count distributions that differ from those reported here, though the fixed-iteration nature of CORDIC limits this sensitivity for trigonometric measurements. Second, the benchmark does not characterize mean absolute error (MAE) for matrix operations; this is deferred to the extended evaluation. Third, the matrix crossover point at  $n \geq 64$  remains a theoretical prediction requiring empirical validation.

## 8 Future Work

### 8.1 Resolving the Matrix Multiplication Crossover (Immediate Priority)

The most urgent item is the empirical characterization of the performance crossover between the Q16.16 tiled kernel and naive floating-point matrix multiplication. The specific questions requiring answers are: at what exact matrix dimension does the tiled Q16.16 kernel first outperform naive float; how does this crossover depend on matrix density and value distribution; and whether reducing the tile size from  $b = 32$  to values matched to the tested dimensions (e.g.,  $b = 8$  or  $b = 16$ ) recovers performance for small matrices. A secondary investigation should determine whether replacing the `int64_t` intermediate accumulator with paired `int32_t` registers reduces register pressure at the cost of a tighter safe operand magnitude constraint.

### 8.2 Branchless CORDIC Quadrant Normalization

The jitter asymmetry in `sin` measurements (coefficient 2.449) is attributable to the conditional branch in the quadrant normalization preprocessor. A branchless normalization using arithmetic shift and masking operations would eliminate this variance and bring the `sin` Determinism Score in line with the 0.994 already achieved by `cos`. This is a single-function optimization estimated at under 10 lines of code with measurable impact on real-time worst-case execution time (WCET) guarantees.

### 8.3 Mean Absolute Error Characterization

The current evaluation characterizes MAE only for scalar operations. A complete precision analysis requires MAE measurement for matrix multiplication across the full range of tested dimensions and input distributions, including the error accumulation behavior as a function of matrix size—predicted to grow as  $O(\sqrt{n})$  for normalized inputs but not yet empirically confirmed on the Xtensa LX6.

## 8.4 Tensor Operations and TinyML Inference

With the matrix multiplication crossover resolved, the natural extension is generalization to rank-3 and rank-4 tensor operations for neural network inference. The Q16.16 multiply-accumulate kernel is mathematically equivalent to the quantized integer kernel used in INT16 inference [11]; the path to a minimal convolutional layer requires only a three-dimensional tiling extension, a bias-addition operation, and a saturating ReLU activation. This targets the precision gap between INT8 inference and IEEE 754 inference documented by [12, 13].

## 8.5 Elliptic Curve Cryptography for Secure Edge Nodes

The field arithmetic underlying ECDSA and X25519—modular addition, modular multiplication, and modular inversion over 256-bit prime fields—maps directly onto the integer pipeline through a multi-limb arithmetic extension [22]. The dual-core architecture is well-suited to this application: scalar multiplication on the elliptic curve is pinned to Core 1 while Core 0 manages the TLS handshake state machine, enabling non-blocking authenticated communication without an external cryptographic coprocessor.

## 8.6 Distributed Multi-Node Linear Algebra

The ESP32’s integrated WiFi controller enables a distributed computation architecture in which multiple nodes partition a large matrix operation across a local network. For matrix dimensions where the single-device Q16.16 kernel is competitive ( $n \geq 64$ ), a mesh of  $k$  ESP32 nodes provides a theoretical  $k$ -fold throughput improvement. The practical characterization of communication overhead versus computation gain constitutes an open research problem at the intersection of distributed systems and embedded computing.

# 9 Conclusion

This paper has presented the design, formal specification, and empirical evaluation of a Dynamic Precision Math Engine for the ESP32 Xtensa LX6 microcontroller. The engine integrates three computational modules—a Q16.16 fixed-point arithmetic core, a 16-iteration CORDIC trigonometric unit, and a cache-aware tiled matrix multiplication kernel—unified by a runtime precision switching mechanism implemented through function pointer dispatch and a two-phase FreeRTOS barrier protocol.

Experimental evaluation across 300 paired measurements on physical hardware produced results that are both significant and instructive. The CORDIC module demonstrated that software architecture can decisively outperform the ESP32’s standard math library for trigonometric computation: median latencies of 293 cycles for `sin` and `cos`—against 6,915 and 7,847 cycles for `sinf()`/`cosf()`—represent speedups of  $18.54\times$  and  $24.68\times$  confirmed at  $p < 10^{-12}$ . The Determinism Score of 0.994 for `cos` establishes that the CORDIC kernel delivers not only speed but predictability, a property of equal value in real-time control systems where worst-case execution time guarantees are required. Scalar Q16.16 multiplication achieved a consistent and perfectly deterministic  $1.5\times$  speedup at 12 cycles versus 18 cycles.

The matrix multiplication results tell a more complex story. The tiled Q16.16 kernel

performed at  $0.54\times$  the speed of naive floating-point for the tested dimensions ( $4\times 4$  through  $16\times 16$ ), revealing that the loop tiling optimization is inert when matrix dimensions fall below the tile size  $b = 32$ . This finding does not invalidate the engine’s design; it precisely defines its operational envelope and validates the necessity of the dynamic precision switch: no single execution path is universally optimal, and the value of the engine lies in making the choice between paths explicit, safe, and costless at the application layer.

The total static memory footprint of 88 bytes and the switch overhead of  $8.09\ \mu\text{s}$  confirm that the engine’s infrastructure cost is negligible for any realistic embedded workload. Beyond the individual algorithms—each with a well-established theoretical basis in the literature of Volder [1], Walther [2], Lam [3], and Goto [5]—the engine’s distinctive contribution is architectural: the application of the separation-of-concerns principle established by the original BLAS specification [4] to the novel context of dynamic precision arbitration on a dual-core RISC microcontroller.

The broader implication of this work is that the performance ceiling of low-cost microcontrollers is not fixed by hardware alone: it is negotiable through principled software architecture. For the class of applications dominated by trigonometric computation—robot kinematics, IMU fusion, angle-based control, DSP—the engine presented here moves the ESP32 into a performance regime previously requiring more expensive hardware, while the identified boundary conditions provide a clear roadmap for future improvement.

## References

- [1] J. E. Volder, “The CORDIC trigonometric computing technique,” *IRE Transactions on Electronic Computers*, vol. EC-8, no. 3, pp. 330–334, Sep. 1959.
- [2] J. S. Walther, “A unified algorithm for elementary functions,” in *Proceedings of the Spring Joint Computer Conference*, vol. 38, pp. 379–385, May 1971.
- [3] M. S. Lam, E. E. Rothberg, and M. E. Wolf, “The cache performance and optimization of blocked algorithms,” in *Proceedings of the 4th International Conference on Architectural Support for Programming Languages and Operating Systems (ASPLOS IV)*, Apr. 1991, pp. 63–74.
- [4] C. L. Lawson, R. J. Hanson, D. R. Kincaid, and F. T. Krogh, “Basic linear algebra subprograms for Fortran usage,” *ACM Transactions on Mathematical Software (TOMS)*, vol. 5, no. 3, pp. 308–323, Sep. 1979.
- [5] K. Goto and R. A. van de Geijn, “Anatomy of high-performance matrix multiplication,” *ACM Transactions on Mathematical Software (TOMS)*, vol. 34, no. 3, art. 12, May 2008.
- [6] V. Kelefouras, A. Kritikakou, I. Mporas, and V. Kolonias, “A high-performance matrix-matrix multiplication methodology for CPU and GPU architectures,” *Journal of Supercomputing*, vol. 72, no. 3, pp. 804–844, 2016.
- [7] D. Llamocca and C. Agurto, “A fixed-point implementation of the expanded hyperbolic CORDIC algorithm,” *Latin American Applied Research*, vol. 37, no. 1, pp. 83–91, Jan. 2007.

- [8] A. S. N. Mokhtar, M. I. Ayub, N. Ismail, and N. G. Nik Daud, "Implementation of trigonometric function using CORDIC algorithms," in *AIP Conference Proceedings*, vol. 1930, no. 1, 2018.
- [9] A. Ait Madi and A. Addaim, "Optimized method for sine and cosine hardware implementation generator, using CORDIC algorithm," *International Journal of Applied Engineering Research*, vol. 13, no. 1, pp. 21–29, 2018.
- [10] W. Sung and K. I. Kum, "Simulation-based word-length optimization method for fixed-point digital signal processing systems," *IEEE Transactions on Signal Processing*, vol. 43, no. 12, pp. 3087–3091, Dec. 1995.
- [11] B. Jacob et al., "Quantization and training of neural networks for efficient integer-arithmetic-only inference," in *Proceedings of the IEEE Conference on Computer Vision and Pattern Recognition (CVPR)*, 2018, pp. 2704–2713.
- [12] R. David et al., "TensorFlow Lite Micro: Embedded machine learning on TinyML systems," in *Proceedings of Machine Learning and Systems (MLSys)*, 2021.
- [13] M. Courbariaux, Y. Bengio, and J. P. David, "BinaryConnect: Training deep neural networks with binary weights during propagations," in *Advances in Neural Information Processing Systems (NIPS)*, 2015.
- [14] S. W. Williams, A. Waterman, and D. A. Patterson, "Roofline: An insightful visual performance model for multicore architectures," *Communications of the ACM*, vol. 52, no. 4, pp. 65–76, Apr. 2009.
- [15] T. Mytkowicz, A. Diwan, M. Hauswirth, and P. F. Sweeney, "Producing wrong data without doing anything obviously wrong!" in *Proceedings of the 14th International Conference on Architectural Support for Programming Languages and Operating Systems (ASPLOS)*, 2009.
- [16] R. G. Lyons, *Understanding Digital Signal Processing*, 3rd ed. Upper Saddle River, NJ: Pearson Education, 2011.
- [17] Espressif Systems, *ESP32 Technical Reference Manual*, Version 4.3. Shanghai, China: Espressif Systems (Shanghai) Co., Ltd., 2020. [Online]. Available: [https://www.espressif.com/sites/default/files/documentation/esp32\\_technical\\_reference\\_manual\\_en.pdf](https://www.espressif.com/sites/default/files/documentation/esp32_technical_reference_manual_en.pdf)
- [18] Espressif Systems, "ESP-DSP library API reference," Read the Docs, 2020. [Online]. Available: <https://docs.espressif.com/projects/esp-dsp/en/latest/>
- [19] Cadence Design Systems, "Xtensa LX6 customizable DPU datasheet," [Online]. Available: <https://ip.cadence.com/uploads/pdf/xtensa-lx-product-brief.pdf>
- [20] R. Yates, "Fixed-point arithmetic: An introduction," *Digital Signal Labs*, Sep. 2020. [Online]. Available: <https://www.digitalsignallabs.com/fp.pdf>
- [21] C. Felton, "A fixed-point introduction by example," *DSPRelated.com*, Apr. 2011. [Online]. Available: <https://www.dsprelated.com/showarticle/139.php>
- [22] E. Rescorla, "The Transport Layer Security (TLS) protocol version 1.3," IETF RFC 8446, Aug. 2018. [Online]. Available: <https://www.rfc-editor.org/rfc/rfc8446>